arXiv:1010.2316v1 [cond-mat.mtrl-sci] 12 Oct 2010

# First principle study of hydrogen behavior in hexagonal tungsten carbide

Xiang-Shan Kong[a], Yu-Wei You[a], C. S. Liu[a,*], Q. F. Fang[a], Jun-Ling Chen[b], G.-N. Luo[b],

[a] *Key Laboratory of Materials Physics, Institute of Solid State Physics, Chinese Academy of Sciences, P. O. Box 1129, Hefei 230031, P. R. China*

[b] *Institute of Plasma Physics, Chinese Academy of Sciences, Hefei 230031, P. R. China*

**Abstract**

Understanding the behavior of hydrogen in hexagonal tungsten carbide (WC) is of particular interest for fusion reactor design due to the presence of WC in the divertor of fusion reactors. Therefore, we use first-principles calculations to study the hydrogen behavior in WC. The most stable interstitial site for the hydrogen atom is the projection of the octahedral interstitial site on tungsten basal plane, followed by the site near the projection of the octahedral interstitial site on carbon basal plane. The binding energy between two interstitial hydrogen atoms is negative, suggesting that hydrogen itself is not capable of trapping other hydrogen atoms to form a hydrogen molecule. The calculated results on the interaction between hydrogen and vacancy indicate that the hydrogen atom is energetically trapped by vacancy and the hydrogen molecule can not be formed in mono-vacancy. In addition, the hydrogen atom bound to carbon is only found in tungsten vacancy. We also study the migrations of hydrogen in WC and find that the interstitial hydrogen atom

[0]*Author to whom correspondence should be addressed. Email address: csliu@issp.ac.cn Tel: 0086-551-5591062

prefers to diffusion along the $\boldsymbol{c}$ axis. Our studies on the hydrogen behavior in WC provide some explanations for the experimental results of the thermal desorption process of energetic hydrogen ion implanted into WC.

## 1. Introduction

The present design for ITER foresees the use of three plasma facing materials: Be for the first wall, W for the divertor and baffle region and CFC for the divertor strike point tiles.[1, 2, 3] The choice of the different materials leads inexorably to the formation of mixed-materials surface.[4] The mixed-materials can change not only the thermo-mechanical properties, but also fuel retention properties of the plasma facing wall, which influence the hydrogen recycling on the plasma facing surface and the tritium inventory in the vacuum vessel. In ITER, for safety reasons, periodic tritium removal will be required before the in-vessel tritium inventory reaches its administrative limit[5], meaning that tritium retention rate strongly affects ITER operation program in the D-T phase. From these considerations, hydrogen uptake and retention in mixed material systems is an important issue for reliable extrapolation of in-vessel tritium retention in ITER. Previous studies have indicated that a WC layer is probably formed on tungsten surface succeeding carbon impurity deposition.[6, 7, 8, 9] Ueda *et al.*[9] found that all the tungsten atoms near the top surface were combined with carbon atoms to form a tungsten carbide layer, which prevented the implanted H from leaving the tungsten and led to blister formation. Hence, as a fundamental study, understanding the hydrogen behavior in WC is of particular interest for fusion reactor design.

In the last decade, to understand the hydrogen behavior in WC, the thermal desorption processes of energetic hydrogen or deuterium ion implanted into WC have been studied by means of the thermal desorption spectroscopy (TDS).[10, 11, 7, 12] Four desorption peaks are observed, which are denoted by Peak 1, Peak 2, Peak 3, and Peak 4, respectively, and described as follows: Peak 1 and Peak 2 observed at the lower temperature region are attributed to the desorption of hydrogen retained in two different interstitial sites, Peak 3 is due to the desorption of hydrogen trapped by carbon vacancy, and Peak 4 is originated from the detrapping of hydrogen bound to carbon. It should be pointed out that the hydrogen concentration bound to carbon is very low and saturated at the initial stage of hydrogen implantation and no hydrogen molecule formation is observed in WC.[13] In addition, Träskelin et al., [14] have used the molecular dynamics simulations to study the hydrogen bombardment of WC surfaces. Even though certain details of the hydrogen trapping in WC have been addressed by experimental and theoretical studies, several questions on the trapping site of hydrogen and the interaction of hydrogen with the carbon or tungsten vacancy in WC are still not clearly understood. Besides, to our best knowledge, the physical mechanism of hydrogen migration in WC has not been investigated until now. In our preceding works [15], we have theoretically investigated the properties of intrinsic defects in WC and revealed the carbon vacancy to be the dominant defect in WC.

In this paper we employ first-principles calculations to study the hydrogen behavior and the interaction of hydrogen with vacancy defect in WC. The stable interstitial sites for hydrogen atom are identified, and the interaction

of double interstitial hydrogen atoms in WC are investigated to understand whether hydrogen atom can be self-trapping or forms a hydrogen molecule directly. The processes of multiple hydrogen absorption into the vacancy are studied to check the possibility for hydrogen occupancy of the vacancy in WC. We also studied the migration of interstitial hydrogen atom in WC and the detrapping of hydrogen from vacancy. Our calculations are expected to reveal the physical mechanism of hydrogen behavior in WC and provide some explanations for the experimental results of the thermal desorption process of energetic hydrogen ion implanted into WC.

## 2. Computation method

The present calculations have been performed within density functional theory as implemented in the Vienna *ab* initio simulation package (VASP) [16, 17]. The interaction between ions and electrons is described by the projector augmented wave potential (PAW) method [18, 19]. Exchange and correlation functions are taken in a form proposed by Perdew and Wang (PW91) [20] within the generalized gradient approximation (GGA). The supercell approach with periodic boundary conditions is used. Two types of hexagonal simulation supercells are used: the smaller one contains 54 atoms (27 carbon atoms and 27 tungsten atoms) with $3 \times 3 \times 3$ unit cells; the larger one contains 128 atoms (64 carbon atoms and 64 tungsten atoms) with $4 \times 4 \times 4$ unit cells. The grids of $k$-points centered at the Gamma point are sampled by $5 \times 5 \times 5$ for 54-atom supercell and $3 \times 3 \times 3$ for the 128-atom supercell. The relaxations of atomic position and optimizations of the shape and size of the supecell are performed with the plane-wave basis sets with the

energy cutoff of 500 eV throughout this work, which was checked for convergence to be within 0.001 eV per atom in the perfect supercell. The structural optimization is truncated when the forces converge to less than 0.1 eV/nm. In addition, the diffusion properties of hydrogen in WC are calculated by the nudged elastic band method with the 54-atom supercell.

The ground-state properties of WC, including equilibrium lattice parameters and bulk cohesive energy, have been calculated in order to compare with experimental and former theoretical data. Results are presented in Table 1. In addition, we obtained the bulk modulus by fitting the volume and calculated cohesive energy to Murnaghan's equation of the state. It can be seen from Table 1 that our results are in agreement with the available experimental and theoretical values.

Firstly, to identify the energy favorable trapping site, the formation energies of single hydrogen atom occupying different interstitial sites in WC are calculated by

$$E_f = E_{tot}^H - E_{tot} - \mu_H, \tag{1}$$

where $E_{tot}$ is the total energy of WC, $E_{tot}^H$ is the total energy of the system with just a hydrogen atom and $\mu_H$ is the hydrogen chemical potential. And then, we use the binding energy to investigate the interaction of double interstitial hydrogen atoms in WC, which is defined as

$$E_b = 2E_{tot}^H - E_{tot}^{2H} - E_{tot}, \tag{2}$$

where $E_{tot}^{2H}$ is the total energy of the WC with two interstitial hydrogen atoms. Here, negative bonding energy indicates repulsion between hydrogen atoms, while positive binding energy means attraction. Lastly, the interaction between hydrogen and carbon or tungsten vacancy is studied by estimation of

the trapping energy. For clarity, below we illustrate the calculated formula only in the case of carbon vacancy, but the calculation formula can be simply applied for tungsten vacancy by replacing carbon by tungsten. Cumulative hydrogen trapping energy of $m$ hydrogen atoms in a carbon vacancy is calculated by using the following expression [26]:

$$E_{tr}^{mH-V_C} = E_{tot}^{mH-V_C} - E_{tot}^{V_W} - m(E_{tot}^{H} - E_{tot}), \tag{3}$$

where $m$ is the number of hydrogen atoms and $E_{tot}^{mH-V_C}$ is the total energy of WC with $m$ hydrogen atoms and a carbon vacancy. Accordingly, the trapping energy $\Delta E_{tr}^{mH-V_C}$ when the number of hydrogen atoms is increased from $m-1$ to $m$ is defined as:

$$\Delta E_{tr}^{mH-V_C} = E_{tot}^{mH-V_C} - E_{tot}^{(m-1)H-V_C} - (E_{tot}^{H} - E_{tot}). \tag{4}$$

## 3. Results and discussion

### *3.1. Single hydrogen atom in WC*

There are ten possible interstitial sites for hydrogen in WC, as shown in Fig. 1. which are denoted by the symbols O, BOC, BOW, TC, TW, BTC, BTW, C, BCC, and BCW, and described as follows. O is the octahedral interstitial sites formed by equivalent three tungsten atoms and three carbon atoms. BOC and BOW are projections of O site on carbon and tungsten basal plane, respectively. TC and TW are two different tetrahedral interstitial sites formed by two different atomic clusters: the former is composed of three carbon atoms and one tungsten atom and the later consists of three tungsten atoms and one carbon atom. Similarly, BTC and BTW are two different hexahedral sites formed by two different atomic clusters: the former

is formed by three carbon atoms and two tungsten atoms, while the later is made up of three tungsten atoms and two carbon atoms. C is midway between the nearest-neighbor tungsten atom and carbon atom. BCC and BCW are the midway between two nearest carbon and tungsten atoms in the dense $\boldsymbol{a}$ direction, respectively. It should be noted that BTC and BTW are also the projection of TC and TW on the carbon and tungsten basal plane, respectively. All configurations with a hydrogen atom in interstitial site are fully relaxed, and two stable hydrogen interstitial configurations are found: one is that the hydrogen atom occupies the BOW site with a formation energy of -0.54 eV, the other is that the hydrogen atom is located in the site near BOC (namely NBOC, Fig. 1) with a formation energy of 0.07 eV. The hydrogen detrapping from BTW and NBOC sites may be responsible for the Peak 2 and Peak 1, respectively. The present results about interstitial site of hydrogen are disagreement with the conclusion of Horikawa and Igarashi [11, 12] that the stable interstitial sites for hydrogen in WC is BTW and BTC. Both of them did not consider other interstitial sites in WC except BTW and BTC. In order to study the effect of supercell size on the stability of hydrogen interstitial configurations, similar calculations have been performed in 54-atom and 128-atom supercell. It is interest to find that changing the supercell size from 128 to 54 slightly affects the formation energies of the hydrogen interstitial, but it does not change final configurations and their relative stability. The relative energy differences between the defect configurations change by at most 0.06 eV. In the following we report only the results obtained from 128-atom supercell calculations, unless clearly stated otherwise.

*3.2. Double interstitial hydrogen atoms in WC*

We now investigate the interaction of double interstitial hydrogen atoms in WC, in order to understand whether hydrogen atom can be self-trapping or forms a hydrogen molecule directly. In the WC, there are distinct sites aligned along the $\boldsymbol{c}$ directions and in the carbon and tungsten basal plane. Hence, according to the above calculated results, we investigate the interaction of interstitial hydrogen atoms in the following cases: (i) the first hydrogen atoms is placed in the BOW site, and the second atom is inserted at other interstitial site in the same tungsten basal plane; (ii) the first hydrogen atom sits in the NBOC site, and the second atom occupies other interstitial site in the same carbon basal plane; (iii) two interstitial hydrogen atoms along the $\boldsymbol{c}$ axis. All relative initial configurations with double interstitial hydrogen atoms are fully relaxed, and eleven final stable configurations are obtained as shown in Fig. 3. The binding energies of these eleven final configurations are calculated using the Eq. 2. The initial and finial distance between two hydrogen atoms and the corresponding binding energies are summarized in Table 2. As shown in Table 2, the distance between two hydrogen atoms increases, and the binding energy are negative in all configurations. They indicate the present of a repulsive interaction when interstitial hydrogen atom is close to each other. It should be noted that the smallest distance between two hydrogen atoms is 0.144 nm, much longer than the bond length of 0.075 nm in hydrogen molecular. In a word, the present results suggest that hydrogen atoms cannot bind together to form a hydrogen molecule in the perfect bulk WC, and thus no hydrogen bubbles.

*3.3. Hydrogen-vacancy interaction in WC*

In order to check the possibility for hydrogen occupancy of the vacancy in WC, which has been predicted experimently and in molecular dynamic simulation [10, 11, 7, 12, 14], we study in this section multiple hydrogen absorption process into the vacancy. In WC, there are two types of vacancy, namely carbon and tungsten vacancy. For the carbon vacancy, there are six equivalent tungsten atoms around the vacancy site as its first-neighbors with a distance of 0.221 nm and six carbon atoms in the carbon basal plane as its second-neighbors with a distance of 0.293 nm. Similar neighbors exist around the tungsten vacancy site: six carbon atom as the first-neighbors and six tungsten atom as the second-neighbors. Therefore, we investigation hydrogen occupancy in carbon and tungsten vacancy, respectively. For clarity, below we illustrate the simulation method only in the case of carbon vacancy, and the similar processes are used in the case of tungsten vacancy. We first examine several possible occupied sites of hydrogen in carbon vacancy and find the most stable site according to the calculated total energy. And then, we bring the hydrogen atom one by one to the vacancy and minimize the energy to find the most stable configurations of $mH - V_C$ complex. In each step, we investigate up to twenty possible configurations based on the most stable configurations of $(m-1)H - V_C$ complex.

The stable configurations for $mH - V_C$ complexes are represented in Fig. 3, and the corresponding trapping energy for the $m$-th hydrogen atom by the $(m-1)H - V_C$ cluster ($\Delta E_{tr}^{mH-V_C}$) as well as the cumulative trapping energy for trapping $m$ hydrogen atoms in a carbon vacancy ($E_{tot}^{mH-V_C}$), calculated by the Eqs. (3) and (4), are listed in Table 3. As shown in Fig. 4 (a) and

(e), the most stable site for single hydrogen atom is to be at an off-vacancy-center position (0.047 nm from the vacancy center). In the $mH - V_C (m > 1)$ complexes, the hydrogen atom prefers to occupy the projection sites of the BCW on the carbon basal plane and forms four W-H bonds with the nearest tungsten atoms with bond length of about 0.21 nm. It should be noted that the hydrogen behavior in carbon vacancy in WC are similar with that in tungsten vacancy in tungsten [27]. This may be one reason that the desorption temperature of Peak 3 are nearly consistent with the temperature of the desorption peak attributed to the desorption of hydrogen trapped by tungsten vacancies in tungsten [7]. As shown in Table 3, the trapping energies of $mH - V_C$ complexes are negative, and the absolute values of the cumulative trapping energy increases with the number of hydrogen atoms until $m = 3$. This indicates that the addition of hydrogen atoms is energetically favorable. For the $4H - V_C$ complex, the trapping energy is positive, and the cumulative energy become less negative than $3H - V_C$. Thus, we make the conclusion that it is energetically favorable for a mono-carbon-vacancy to trap as many as 3 hydrogen atoms. It should be pointed that the lowest distance between two hydrogen atoms in stable $mH - V_C$ complexes is 0.166 nm, much longer than the bond length of hydrogen molecule, implying that hydrogen atoms cannot bind together to form a hydrogen molecule in mono-carbon-vacancy.

Figure 4 represents the most stable configurations of $mH - V_W$ complexes obtained following the aforementioned method, and Table 4 list the corresponding trapping energy and cumulative trapping energy. In tungsten vacancy, a single hydrogen atom prefers to occupy the interstitial C site to form a C-H bond with the nearest carbon atom with the bond length of

0.116 nm. In $mH - V_W (m > 1)$ complexes, the hydrogen atoms sit in the C and BOW around the vacant site, and detailed structural properties are summarized in Table 4, such as the occupancy sites of $m$ hydrogen atoms, the number and length of the C-H bonds, and the smallest distance between two hydrogen atoms in $mH - V_W$ cluster. As shown in Table 4, the trapping energy varies slowly at first but then very rapidly becomes less negative with the increasing the number of hydrogen atoms up to 9, beyond which the trapping energy becomes positive. In addition, the cumulative trapping energy increases in its absolute value with the number of hydrogen atoms in $mH_W$ cluster until $m = 9$. Thus, we suggest that the maximum number of hydrogen atoms are trapped by mono-tungsten-vacancy is 9. Note that, in all stable $mH - V_W$ clusters, the H-H distance are much larger than the bond length of $H_2$, indicating that the hydrogen molecule can not be formed in mono-tungsten-vacancy. In addition, there are as many as 6 C-H bonds in a tungsten vacancy. It should be pointed out that the hydrogen atoms bound to carbon are only found in tungsten vacancy whose concentration in WC is very small. This is why the concentration of hydrogen bound to carbon in WC is very low [7].

### *3.4. Migration of interstitial hydrogen atom in WC*

Concerning the kinetics of hydrogen in WC, we first examine the case of interstitial hydrogen migration, which is relevant to the initial stage after hydrogen implantation or low temperature re-emission of hydrogen atoms trapped in WC. As shown in Fig. 5, we investigate four routes named by Path A, Path B, Path C and Path D, respectively. Path A ($4 \rightarrow 5$) is the migrate of hydrogen atom between two nearest equivalent BOW site with

the energy barrier of 1.79 eV; Path B ($1 \rightarrow 2$) and Path C ($2 \rightarrow 3$) are the diffusions of hydrogen atom in carbon basal plane: the former is the diffusion of hydrogen atom between two nearest-neighbor NBOC sites around the same BOC site with a barrier energy of 0.23 eV, while the later is that around different BOC site with a large energy barrier of 0.84 eV. Path D ($1 \rightarrow 4$) propagates parallel to the $\boldsymbol{c}$ direction, and the energy barrier of hydrogen jumping from the NBOC to the nearest BOW is 0.05 eV, while the reverse diffusion energy barrier is 0.5 eV. Therefore, the interstitial hydrogen atom prefers to jump form NBOC to BOW along the $\boldsymbol{c}$ axis in WC.

We now turn to the kinetic process for hydrogen detrapping from carbon vacancy in WC. Similarly, we investigate two diffusion routes for hydrogen detrapping from carbon vacancy shown in Fig. 6: one is that hydrogen atom diffusion in the carbon plane ($1 \rightarrow 2$, Path E); the other is parallel to the $\boldsymbol{c}$ axis ($1 \rightarrow 3 \rightarrow 4$, Path F). For path E, the energy barrier for hydrogen atoms jumping away from the carbon vacancy is 2.1 eV, which are greatly lager than the corresponding reverse energy barrier (0.73 eV). Path F involves two steps for hydrogen detrapping from carbon vacancy. The first step is that hydrogen atom jump form site 1 to 3 with a diffusion barrier of 0.64 eV, and the second step is hydrogen diffuse from site 3 to 4 with a energy barrier of 1.06 eV. Not that, in both Path E and Path F, the hydrogen detrapping energy barrier are much larger than hydrogen tapping energy barrier. This means that the hydrogen atom is energetically trapped by the carbon vacancy. It should be pointed out that the energy barrier of interstitial hydrogen diffusion near the carbon vacancy becomes smaller than that in the area without carbon vacancy.

As similar as the case of hydrogen detrapping from carbon vacancy, we study two diffusion routes for hydrogen detrapping from tungsten vacancy shown in Fig. 7: one is that hydrogen diffusion in the tungsten basal plane ($1 \rightarrow 2 \rightarrow 3$, Path G); the other propagates along the $\boldsymbol{c}$ axis ($1 \rightarrow 2 \rightarrow 4$, Path J). Both of them involve the step that hydrogen atom jumps from C site to the BOW in tungsten vacancy with the energy barrier of 0.58 eV. For Path G, the energy barrier of hydrogen atoms jumping away from the tungsten vacancy is 3.88 eV, greatly larger than that along the $\boldsymbol{c}$ axis. It should be noted that the energy barrier of hydrogen atom jumping into the tungsten vacancy is relatively low. Together with the low concentration of hydrogen bound to carbon vacancy, may provide an explanation for that the concentration of hydrogen bound to carbon is saturated at the initial stage of hydrogen implantation [7].

## 4. conclusion

We use first-principles calculations to study the hydrogen behavior in WC. Two stable interstitial sites for hydrogen atoms, namely BOW and NBOC. BOW is more stable for interstitial hydrogen atoms than NBOC. The binding energy between two interstitial hydrogen atoms is negative, suggesting that hydrogen itself is not capable of trapping other hydrogen atoms to form a hydrogen molecule. The calculated results on the interaction between hydrogen and vacancy indicate that the maximum number of hydrogen atoms trapped by mono-carbon-vacancy and mono-tungsten-vacancy are 3 and 9, respectively, and the hydrogen molecule can not be formed in mono-carbon-vacancy and mono-tungsten-vacancy. It should be noted that the hydrogen

atoms bound to carbon are only found in tungsten vacancy whose concentration in WC is very small. This is why the concentration of hydrogen bound to carbon in WC is very low. We also investigate the migration of hydrogen in WC with and without vacancy defect. The calculated results suggest that the interstitial hydrogen atom prefers to diffusion along the $\boldsymbol{c}$ axis, and the hydrogen atom are easily diffusion into and trapped by the vacancy. It should be pointed out the energy barrier of the hydrogen atom jumping into the tungsten vacancy is very low. This provides an explanation for that the concentration of hydrogen bound to carbon is saturated at the initial stage of hydrogen implantation in WC.

**Acknowledgement**

This work was supported by the National Magnetic Confinement Fusion Program (Grant No.: 2009GB106005) and the Innovation Program of Chinese Academy of Sciences (Grant No.: KJCX2-YW-N35), and by the Center for Computation Science, Hefei Institutes of Physical Sciences.

**References**

[1] M. Kaufmann and R. Neu, Fus. Eng. Des. 82, (2007) 521.

[2] J. Pamela, G. F. Matthews, V. Philipps, and R. Kamendje, J. Nucl. Mater. 363-365,(2007) 1.

[3] R. P. Doerner, J. Nucl. Mater. 363-365, (2007) 32.

[4] A. Loarte, B. Lipschultz, A.S. Kukushkin, et al., Nucl. Fusion 47 (2007) S203.

[5] G. Federici, R.A. Anderl, P. Andrew, et al., J. Nucl. Mater. 266C269 (1999) 14.

[6] W. Eckstein and J. Roth, Nucl. Instrum. Meth. B 53, (1991) 279.

[7] H. Kimura, Y. Nishikawa, T. Nakahata, M. Oyaidzu, Y. Oyab, and K. Okunoa, Fus. Eng. Des. 81, (2006) 295.

[8] K. Sugiyama, K. Krieger, C. P. Lungu, and J. Roth, J. Nucl. Mater. 390-391, (2009) 659.

[9] Y. Ueda, T. Shimada, M. Nishikawa, Nucl. Fusion 44 (2004) 62.

[10] T. Horikawa, B. Tsuchiya, and K. Morita, J. Nucl. Mater. 258-263, (1998) 1087.

[11] T. Horikawa, B. Tsuchiya, and K. Morita, J. Nucl. Mater. 266-269, (1999) 1091.

[12] E. Igarashi, Y. Nishikawa, T. Nakahata, A. Yoshikawa, M. Oyaidzu, Y. Oya, and K. Okuno, J. Nucl. Mater. 363-365, (2007) 910.

[13] O. V. Ogorodnikova, J. Roth, and M. Mayer, J. Nucl. Mater. 313-316, (2003) 469.

[14] P. Träskelin, N. Juslin, P. Erhart, and K. Nordlund, Phys. ReV. B 75, (2007) 174113.

[15] X.S. Kong, Y.W. You, J.H. Xia, C.S. Liu, Q.F. Fang, G.-N. Luo, Q.Y. Huang, J. Nucl. Mater. (2010), doi:10.1016/j.jnucmat.2010.09.002.

[16] G. Kresse and J. Hafner, Phys. Rev. B 47, (1993) 558.

[17] G. Kresse and J. Furthmüler, Phys. Rev. B 54, (1996) 11169.

[18] G. Kresse and D. Joubert, Phys. Rev. B 59, (1999) 1758.

[19] P. E. Blöchl, Phys. Rev. B 50, (1994) 17953.

[20] J. P. Perdew, J. A. Chevary, S. H. Vosko, K. A. Jackson, M. R. Pederson, D. J. Singh, and C. Fiolhais, Phys. Rev. B 46, (1992) 6671; 48, (1993) 4978(E).

[21] H. J. Monkhorst, and J. D. Pack, Phys. Rev. B 13, (1976) 5188.

[22] H. O. Pierson, *Handbook of Refractory Carbides and Nitrides: Properties Characteristics, Processing, and Applications Noyes*, Westwood, NJ, 1996.

[23] H. L. Brown, P. E. Armstrong, and C. P. Kempter, J. Chem. Phys. 45, (1966) 547.

[24] D. R. Lide *Handbook of Chemistry and Physics*, 85th ed. (CRC, Boca Raton, 2004).

[25] N. Juslin, P. Erhart, P. Träkelin, J. Nord, K. O. E. Henriksson, K. Nordlund, E. Salonen, and K. Albe, J. Appl. Phys. 98, (2005) 123520.

[26] O. Yu. Vekilova, D. I. Bazhanov, S. I. Simak, and I. A. Abrikosov, Phys. Rev. B 80, (2009) 024101.

[27] Y. L. Liu, Y. Zhang, H. B. Zhou, G. H. Lu, F. Liu, and G. N. Luo, Phys. Rev. B 79, (2009) 172103.

Table 1 The bulk properties and cohesive energy ($E_c$) of WC, MD and DFT mean the results obtained by molecular dynamic simulation and density functional theory, respectively.

| | $a_0$(nm) | $c_0/a_0$ | $B_0$(GPa) | $E_c$(eV) |
|---|---|---|---|---|
| Experiment | 0.2907[a] | 0.976[a] | 329[b] | -16.68[c] |
| MD[d] | 0.2917 | 0.964 | 443 | -16.68 |
| DFT[d] | 0.2979 | 0.975 | 368 | -15.01 |
| Present work | 0.2932 | 0.973 | 356 | -16.42 |

[a] Reference [22]

[b] Reference [23]

[c] Reference [24]

[d] Reference [25]

Table 2 The initial and final distance (before and after the relaxation, nm) between two hydrogen atoms and corresponding binding energy (eV) in three cases.

| case | Site of second atom | Initial distance | Final distance | Bonding energy |
|---|---|---|---|---|
| (i) | 1 | 0.1681 | 0.1743 | -1.92 |
| | 2 | 0.2906 | 0.2971 | -0.18 |
| | 3 | 0.5033 | 0.5093 | -0.06 |
| | 4 | 0.5812 | 0.5875 | -0.06 |
| (ii) | 1 | 0.1163 | 0.1444 | -0.59 |
| | 2 | 0.2932 | 0.2983 | -0.11 |
| | 3 | 0.3467 | 0.3503 | -0.09 |
| | 4 | 0.3849 | 0.3856 | -0.07 |
| | 5 | 0.5865 | 0.5866 | -0.05 |
| (iii) | 1 | 0.2838 | 0.2920 | -0.17 |
| | 2 | 0.5674 | 0.5721 | -0.02 |

Table 3 The trapping energy for the $m$-th hydrogen atom by the $(m-1)H-V_c$ cluster ($\Delta E_{tr}^{mH-V_C}$, eV) and the cumulative trapping energy for trapping $m$ hydrogen atoms in a carbon vacancy ($E_{tot}^{mH-V_C}$, eV).

| system | $\Delta E_{tr}^{mH-V_C}$ | $E_{tot}^{mH-V_C}$ |
|---|---|---|
| $1H-V_C$ | -0.25 | -0.25 |
| $2H-V_C$ | -0.83 | -1.08 |
| $3H-V_C$ | -0.27 | -1.35 |
| $4H-V_C$ | 0.20 | -1.15 |

Table 4 The trapping energy for the $m$-th hydrogen atom by the $(m-1)H-V_W$ cluster ($\Delta E_{tr}^{mH-V_W}$, eV) and the cumulative trapping energy for trapping $m$ hydrogen atoms in a tungsten vacancy ($E_{tot}^{mH-V_W}$, eV). $N_{C-H}$ and $D_{C-H}$ (nm) are the number and length of C-H bond, respectively. $D_{H-H}$ (nm) is the smallest distance between two hydrogen atoms.

| system | Occupied site | $\Delta E_{tr}^{mH-V_W}$ | $E_{tot}^{mH-V_W}$ | $N_{C-H}$ | $D_{C-H}$ | $D_{H-H}$ |
|---|---|---|---|---|---|---|
| $1H-V_W$ | 1 | -0.95 | -0.95 | 1 | 0.116 | |
| $2H-V_W$ | 1,2 | -0.89 | -1.85 | 2 | 0.115 | 0.224 |
| $3H-V_W$ | 1∼3 | -0.93 | -2.78 | 2 | 0.116 | 0.178 |
| $4H-V_W$ | 1∼4 | -0.92 | -3.70 | 2 | 0.116 | 0.174 |
| $5H-V_W$ | 1∼5 | -0.95 | -4.66 | 2 | 0.116 | 0.175 |
| $6H-V_W$ | 1∼6 | -0.70 | -5.36 | 3 | 0.117 | 0.153 |
| $7H-V_W$ | 1∼7 | -0.62 | -5.97 | 4 | 0.114 | 0.155 |
| $8H-V_W$ | 1∼8 | -0.07 | -6.04 | 5 | 0.114 | 0.149 |
| $9H-V_W$ | 1∼9 | -0.01 | -6.05 | 6 | 0.111 | 0.149 |
| $10H-V_W$ | 1∼9,sub | 1.48 | -4.57 | 6 | 0.113 | 0.129 |

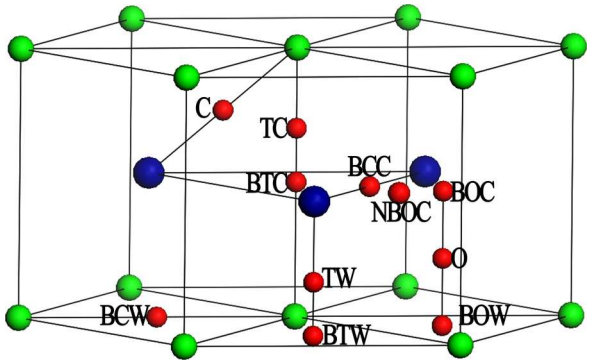


Figure 1: (color online)Schematic diagram of various isolated interstitial sites in WC. The tungsten and carbon atoms are marked in green (white) and blue (black) balls, respectively. The small red (dark gray) balls represent the interstitial sites.

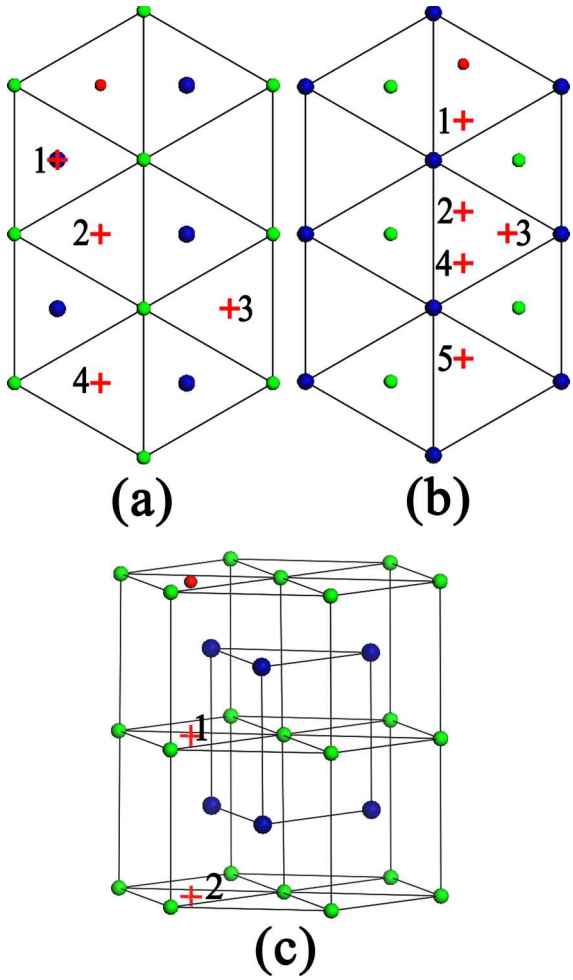


Figure 2: (color online) The final stable configurations of double interstitial hydrogen atoms in WC. The (a), (b) and (c) show the final configurations of case (i), (ii) and (iii), respectively. The tungsten and carbon atoms are marked in green (white) and blue (black) balls, respectively. The small red (dark gray) balls represent the first interstitial hydrogen atom, and the red '+', named by $1 \sim 5$, denotes the sites occupied by the second hydrogen atom.

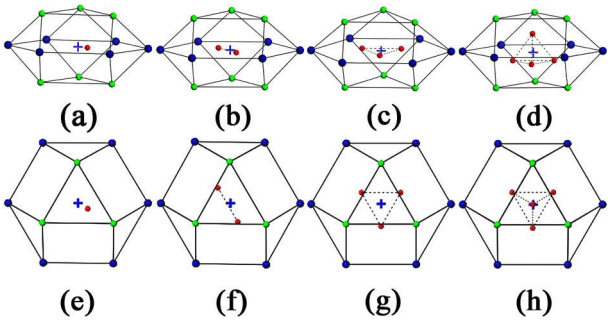


Figure 3: (color online) Schematic representation of the lowest-energy configurations $mH-V_C$: (a) $1H-V_C$, (b) $2H-V_C$, (c) $3H-V_C$, (d) $4H-V_C$. The (e)$\sim$(f) are top-view images of (a)$\sim$(d), respectively. The tungsten, carbon and hydrogen atoms are marked in green (white), blue (black), and red (gray) balls, respectively. The green '+' represents the carbon vacancy site.

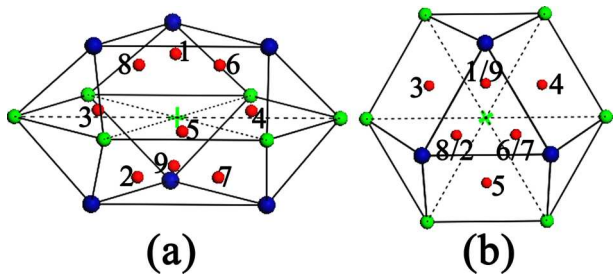


Figure 4: (color online) Schematic representation of the lowest-energy configurations $mH-V_W$. The (b) is top-view images of (a). The tungsten and carbon atoms are marked in green (white) and blue (black), respectively. The blue '+' represents the tungsten vacancy site. The sites occupied by the hydrogen atoms are marked by the red balls, named by 1∼9, respectively.

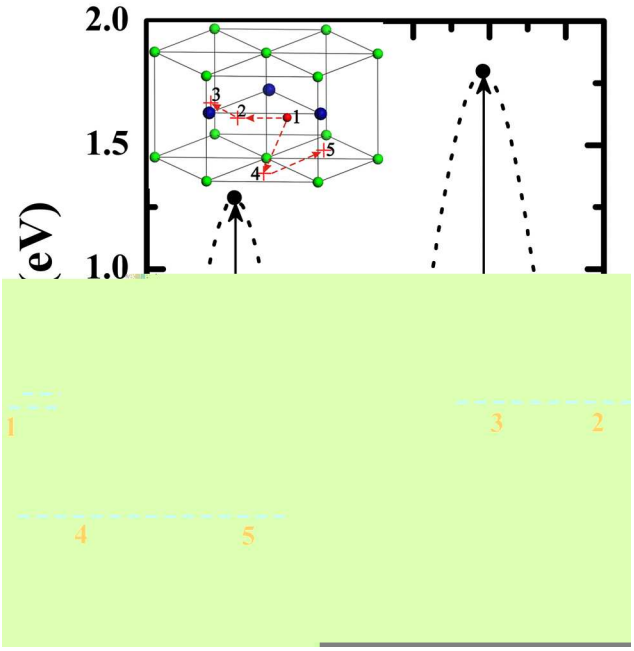


Figure 5: (color online) Diffusion energy profile and the corresponding diffusion paths for interstitial hydrogen atom in WC. The tungsten and carbon atoms are marked in green (white) and blue (black), respectively. Site 1, 2 and 3 are the different NBOC sites in a carbon basal plane and Sites 4 and 5 are two nearest BOW sites in a tungsten basal plane.

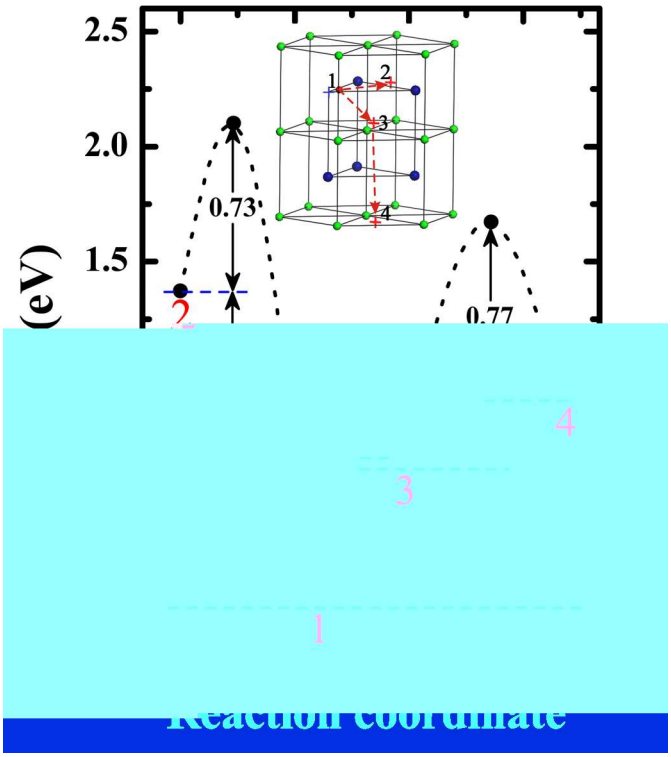


Figure 6: (color online) Hydrogen diffusion energy profile and the corresponding diffusion paths around the carbon vacancy in WC. The tungsten, carbon and hydrogen atoms are marked in green (white), blue (black), and red (gray) ball, respectively. The green '+' represents the carbon vacancy site. The red '+' are the relative stable sites of hydrogen. Site 1 is the most stable site of hydrogen in carbon vacancy. Sites 2 and 3 are the first nearest neighbor NBOC and O site of the carbon vacancy, respectively. Site 4 is the second nearest neighbor BOW site of the carbon vacancy.

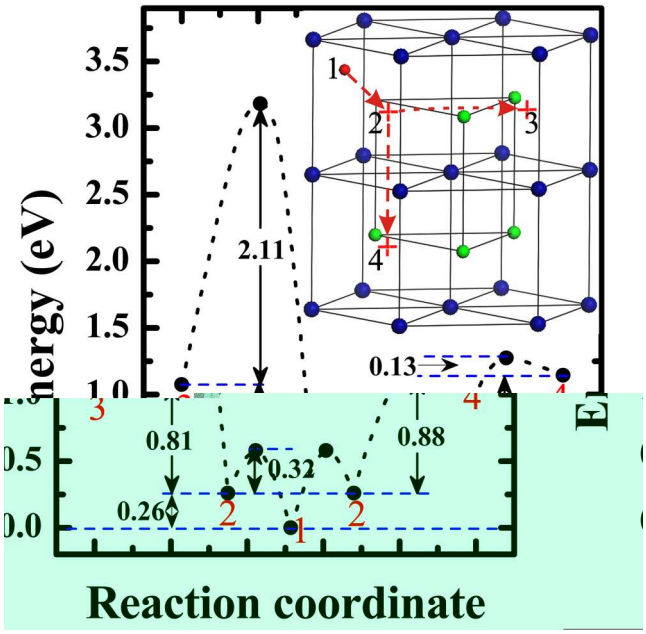


Figure 7: (color online) Hydrogen diffusion energy profile and the corresponding diffusion paths around the tungsten vacancy in WC. The tungsten, carbon and hydrogen atoms are marked in green (white), blue (black), and red (gray) ball, respectively. The blue '+' represents the tungsten vacancy site. The red '+' are the relative stable sites of hydrogen. Site 1 is the most stable site of hydrogen in tungsten vacancy. Site 2 is the BOW sites in tungsten vacancy. Sites 3 and 4 are the nearest BOW site of site 2 along the c direction and in same tungsten basal plane, respectively.